DAIS LARGE SCALE FACILITY

RESEARCH PROJECT

DAIS-96-ES3

REMVEG:
REMOTE ASSESSMENT OF VEGETATION STATUS BY HYPERSPECTRAL IMAGERY

PROGRESS REPORT

AUTHORS:

Agustín Lobo (1), Nicolau Pineda (1), José-Luis Fernández-Turiel (1), Josep Peñuelas (2), Iolanda Filella (2), Romà Ogaya (2), Victoria Cachorro (3), A.M. de Frutos (3)

(1) Institut de Ciències de la Terra (Consejo Superior de Investigaciones Científicas).
(2) CREAF, Universitat Autònoma de Barcelona.
(3) Departamento de Óptica y Física Aplicada, Universidad de Valladolid.

CONTACT:

Agustín Lobo

Institut de Ciències de la Terra (CSIC)

Lluis Solé Sabaris s/n, 08028 Barcelona (Spain)

Phone 34-93-3302716

Fax: 34-93-4110012

e-mail:alobo@ija.csic.es

INDEX

1.INTRODUCTION

Broad-band, high-spatial resolution satellite Remote Sensing (i.e., Landsat-TM, Spot-HIV) has proved to be an essential tool for landcover change mapping, but insufficient to (i) resolve subtle categories like the ones often needed for ecological research, and (ii) measure biophysical magnitudes. Narrow-band hyper-spectral airborne Remote Sensing provides data that can be used for these purposes, but also generates specific processing needs. Classical multivariate clustering techniques and simple vegetation indexes, traditionally applied to broad-band satellite imagery, are insufficient to retrieve information from narrow-band hyper spectral imagery. The processing of this imagery needs (i) to be driven from dedicated field data, in particular from field spectroscopy and (ii) to abandon the pixel as the processing unit and to substitute it by patches, as produced by segmentation algorithms (Lobo 1997).

Within the frame of our general goals in the project, we have focused on the evaluation of DAIS imagery to (i) characterize different vegetation covers in terms of their hyperspectral signatures and to (ii) use the DAIS signatures to assess vegetation condition in a parallel way as this has been previously done with hand-held field spectro-radiometry (Gamon et al. 1992, Peñuelas et al. 1995).

We describe in this intermediate report our first steps and results processing DAIS hyperspectral imagery acquired over a humid Mediterranean forest in Les Gavarres (NE Spain, 41° 54' N, 2° 58' E).

2.CAMPAIGN PLANING

2.1 Area of study

Les Gavarres is a Mediterranean forest area (ca. 250 km^2) in Catalonia (NE Spain), between the city of Girona and the Costa Brava tourist area. Les Gavarres is an old (Hercynian), small mountain range of low altitude (maximum height is 535 m) essentially made of sedimentary and vulcano-sedimentary rocks.

Click on image for full resolution.

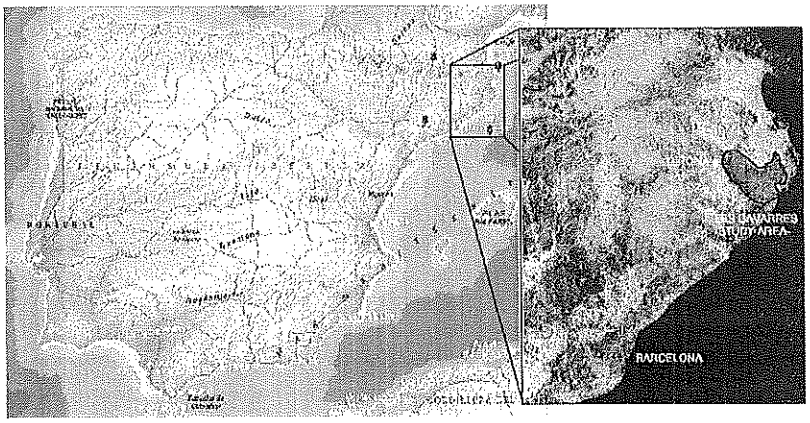

Figure 1: Geographic location of our area of study

Climate is humid Mediterranean, with 600 – 800 mm of annual precipitation and 14°; C of annual mean temperature. Summer is dry but the drought period (defined as the period with potential evapotranspiration higher

than precipitation) is short.

Click on image for full resolution.

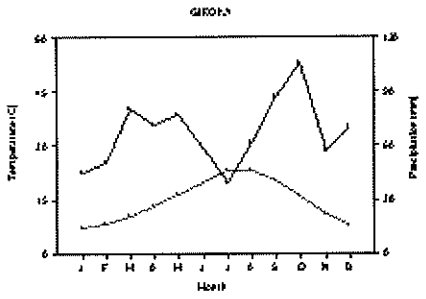

Figure 2: Mean monthly temperature and precipitation of Girona

Vegetation has a 100% cover and is dominated by evergreen oaks (*Quercus suber* and *Q. ilex*) with an important presence of pines (*P. pinaster, P. pinea* and *P. halepensis*), with well developed riparian forest along the streams and patches of *Castanea sativa* in the most humid zones. There are also some plantations of *Eucalyptus sp.* As typical in Mediterranean forests, shrubs have an important cover (*Arbutus unedo, Pistacia lentiscus, Erica arborea, Cistus monspeliensis*...) as understorey, and dominate in degraded areas or after disturbance.

Click on image for full resolution.

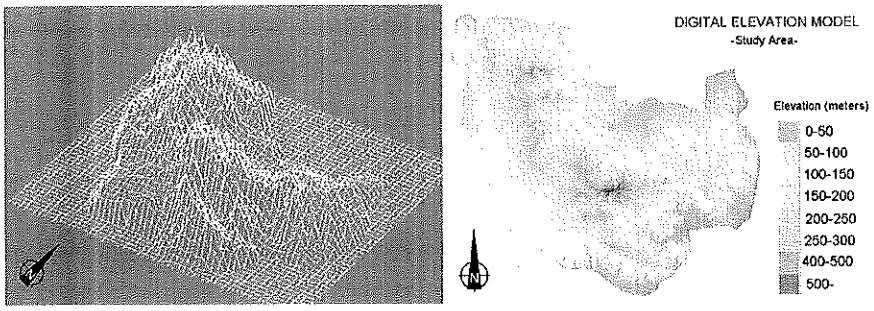

Figure 3: Topography of the area in 3D (left) and 2D (right).

The most important traditional economic value of Les Gavarres was the production of cork. Nowadays, the direct economic interest od the forest is relatively low compared to profits on the nearby tourist coast. Neverthelss, the area has an important potential role for tourism because its environmental and historical values in the vicinity of the Costa Brava. The abandonment of traditional practices has made this Mediterranean forest highly combustible and forest management is practically reduced to fire suppression. A correct evaluation of ecological forest variables, in particular water stress, is an important challenge for environmental remote sensing in this area as a basic information for environmental management.

2.2. Basic description of DAIS

DAIS (Digital Airborne Imaging Spectrometer) is a 79 channel high resolution optical spectrometer which collects information from Earth's surface in the 0.14 – 12.3 μm wavelengths region. Table 1 provides the essential technical information. See http://www.op.dlr.de/DAIS/dais-scr.htm for an extended information.

Table 1: Spectral band specifications, main radiometric, and geometric instrument parameters of the DAIS 7915

(from "The DAIS 7915 System Specifications" in http://www.op.dlr.de/DAIS/dais- scr.htm **by** Peter.Strobl@DLR.DE)

Spectrometer Characteristics

(Wavelength range: 400nm - 12.6μm, 4 Spectrometers, 79 bands)

1) 400 - 1000 nm : 32 Bands, Bandwidth = 15-30 nm Detector: Si

2) 1500 - 1800 nm : 8 Bands, Bandwidth = 45 nm Detector: InSb

3) 2000 - 2500 nm : 32 Bands, Bandwidth = 20 nm Detector: InSb

3000 - 5000 nm : 1 Band , Bandwidth = 2.0 μm Detector: InSb

4) 8000 -12600 nm : 6 Bands, Bandwidth = 0.9 μm Detector: MCT

Main radiometric parameters

Dynamic range: 15 bit (no gain settings)
Sensitivity VIS/NIR: NER < 0.025 mW/cm^2 sr μm
SWIR: NER < 0.025 mW/cm^2 sr μm
MIR/TIR: NET < 0.1 K

Main geometric parameters

FOV: 0.894 rad (+-26 degrees) on DO 228,
depending on aircraft max.+- 39
IFOV: 3.3 mrad, (0.189 degrees)
GIFOV: depending on aircraft altitude 5 - 20 m
Scan frequency: adjustable according to aircraft altitude
between 6 and 24 Hz Image pixels per line: 512

2.3 Flight lines

We set up three flight lines of 3.3 km x 12 km that intersected most vegetation types according to previous information. In order to minimize the variation of sun angle along lines in the image, flight lines were set to direct the airplane towards the sun, that is, to keep an small angle between the nadir (central) column and the sun. The actual location of our planned flight lines is represented in Fig.4.

Click on image for full resolution.

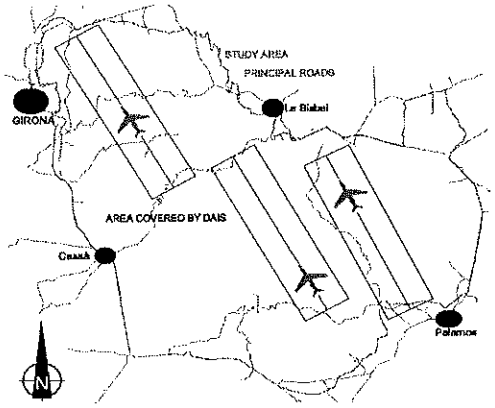

Figure 4: Planned flight lines and over the map (UTM zone: 31).

3.CAMPAIGN

3.1. Field spectro-radiometry

Spectra of vegetation were acquired in the field with a Spectron SE-590 spectroradiometer and halon reference. Spectra were acquired for leaves and branches of *Pinus halpensis, P. pinea, Quercus suber, Q. ilex, Erica arborea, Cistus monspeliensis* and *Castanea sativa.*

Click on image for full resolution.

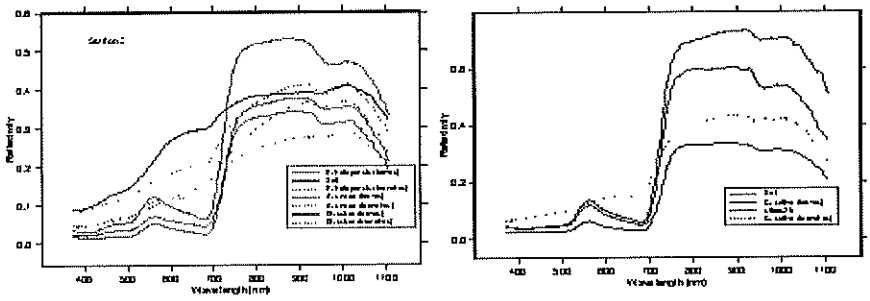

Figure 5. Some field-collected reflectance spectra.

In addition, samples of these species were taken to measure their water content. The physiological reflectance index (PRI) and water reflectance index (WI) were calculated from the spectra as:

$$\mathbf{PRI = (R570 - R531)/(R570 + R531)}$$

$$\mathbf{WI = R900/R970}$$

Where R stands for reflectance and the numbers for wavelengths in nm.

Click on image for full resolution.

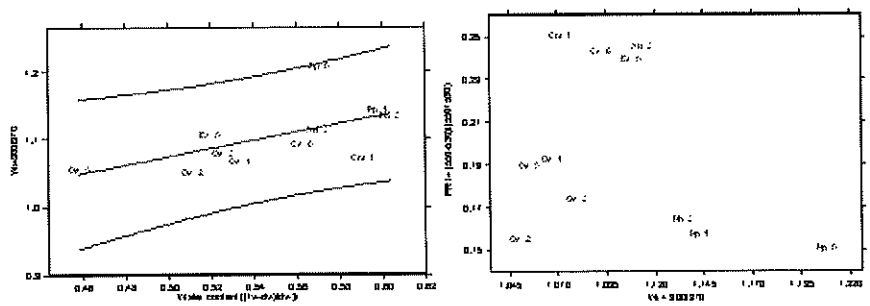

Figure 6. Left, relationship of WI to water content. Right, the field-collectedspectra in the plane defined by PRI and WI.

3.2. Atmospheric measurements

We acquired a total of 6 spectra of direct normal solar irradiance and 3 of global horizontal irradiance between 300-1100 nm with a Licor 1800 spectroradiometer. We used these spectra to determine the total optical depth and atmospheric transmittance, and to derive the aerosol optical depth, ozone and water vapor content. Three spectra of vertical downward radiance were also measured to derive the aerosol phase function.

The aerosol optical depth was calculated from measured direct solar irradiance according to Cachorro et al. (1995). The spectral optical depth of aerosols was used to calculate the distribution function of aerosol sizes based on the theory of Mie and assuming a log-normal distribution. The phase function and the skewness parameter were calculated from the distribution (Cachorro et al 1997.)

As no portable equipment for radio-sounding was available, we only can use the data acquired at the airport of Palma de Mallorca, which have been provided by the Instituto Nacional de Meteorología.

Click on image for full resolution.

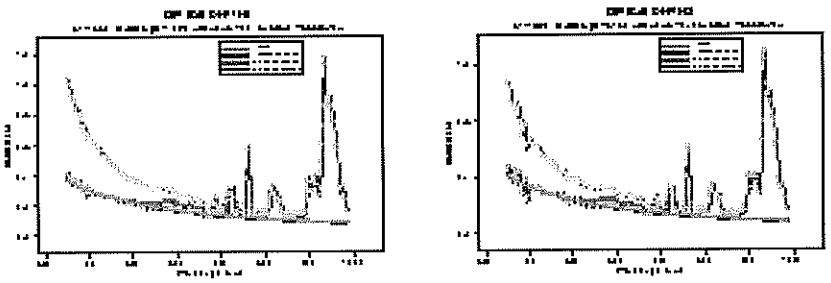

Figure 7. Spectra for optical depths measured in Les Gavarres during the campaign.

3.3. Imagery

The following images (Table 2) were acquired over our study area on 9 – July– 1997. We selected the three scenes that were acquired between 11:06 and 11:33 a.m. because of their better atmospheric conditions.

TABLE 2. Scenes acquired from The DAIS 7915 Large-Scale Facility, (Es3).

DATE	TITLE	C	TIME	ALT.	HED.	SF	ROWS	COMMENT	QLOOK
970709	ES3_1	1	10:52	3200	333	11	2478	start too early	p01i03c1h11_f01_raw
970709	ES3_1	1	11:06	3200	335	12	2478	Repetition **SELECTED**	p02i02c1h12_f02_raw
970709	ES3_2	1	11:20	3200	331	12	2454	Hazy **SELECTED**	p03i02c1h12_f03_raw
970709	ES3_3	1	11:33	3200	127	12	2478	scattered clouds **SELECTED**	p04i02c1h12_f04_raw
970709	ES3_3	1	12:35	3200	325	12	2478	scattered clouds	p05i02c1h12_f05_raw
970709	ES3_2	1	12:52	3200	326	12	2478	cloud shadows	p06i02c1h12_f06_raw
970709	ES3_1	1	13:07	3200	331	13	2478	last 200 lines corrupt	p07i02c1h13_f07_raw

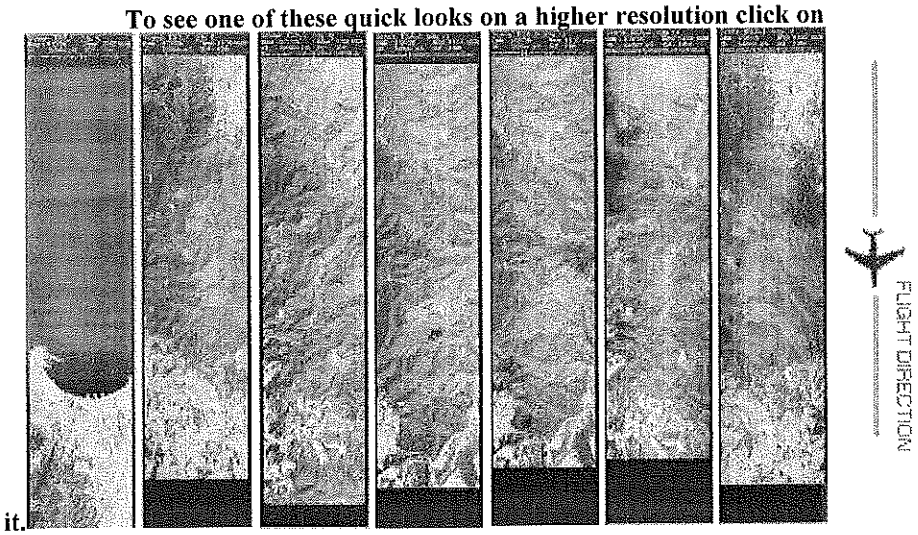

Figure 8. Quicklooks of the scenes listed in Table 2.

Images were provided by the DAIS processing team as calibrated at-sensor radiances in 0.001 * mW/(sr*cm^2;* μm) for bands 1-72 and 0.0001* mW/(sr*cm^2;*μm) for bands 74-79. A description of the calibration methods can be obtained in http://www.op.dlr.de/DAIS/dais-cal.htm and http://www.op.dlr.de/dais/dais-prc.htm .

An auxiliary database in IDL XDR (eXternal Data Representation) format contained information on flight parameters. Unfortunately, essential information for users, such are view zenithal and azimuthal angles, and ground resolution, are not in the database, although the database contains the necessary lower-level parameters for the users to make their own computations.

In our case, a mechanical failure of auxiliary DAIS instrumentations made that PIT angles were not recorded and we had to estimate them from the records of the airplane navigation instruments.

The general quality of the scenes was good, although some bands presented a notorious stripping. Here we present the bands of the p02i02c1h12_f02.bsq scene. The composition has been produced with MOSAICO, an IDL/ENVI application that we have developped for a quick inspection of hyper-spectral imagery and made publicaly available.

Click on the mosaic to see 3 detailed mosaics of bands 1-79, 1-32 and 66 - 79

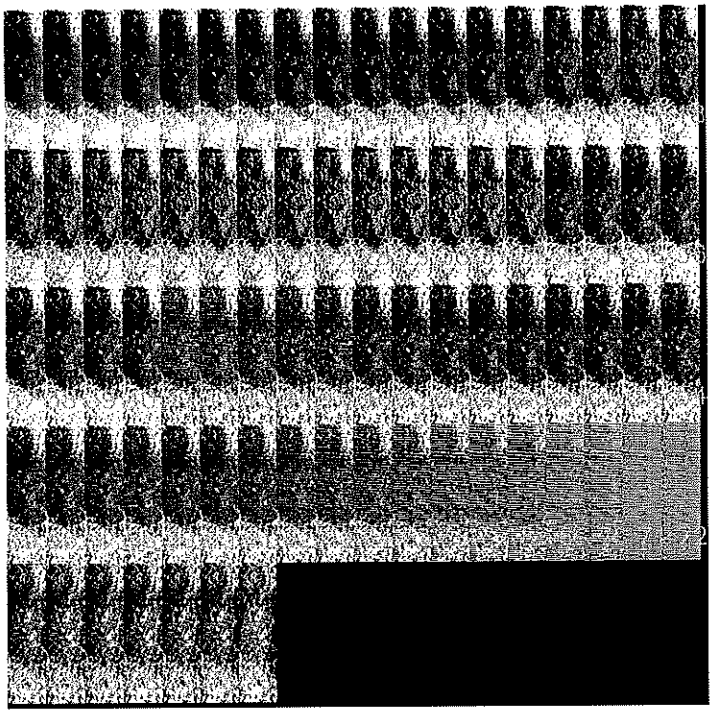

Figure 9. Mosaics of the bands of the p02i02c1h12_f02.bsq scene

Table 2. ATREM water-vapor parameters for DAIS imagery (vegetated scenes)

	Window 1		Window 2		Absorption	
	Center (nm)	Width (# bands)	Center (nm)	Width (# bands)	Center (nm)	Width (# bands)
"940 band"	860	1	1034	1	947	1
"1140 band"	860	1	1034	1	947	1

where we must note the following differences to the above mentioned values for AVIRIS:

- The two lines are the same because DAIS lacks bands in the 1140 nm region.
- Wavelengths are slightly modified to match the centers of the nearest bands for DAIS.
- Single bands instead of averages are used because DAIS spectral bands are wider.

With these parameters, ATREM produced the following water vapor image for our first selected scene (p02i02c1h12_f02.bsq)

Click on image for full resolution.

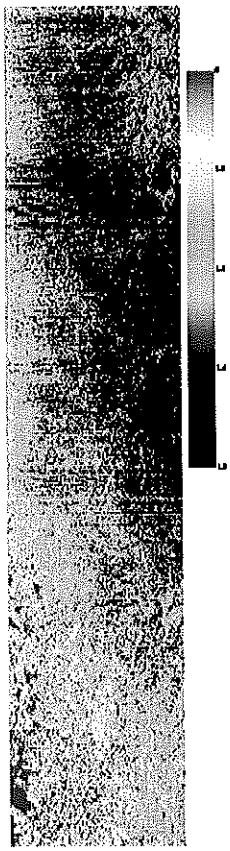

Figure 11. Image of water vapor calculated by ATREM (in cm).

4.PROCESSING

4.1. Signal to noise ratio

We made an assessment of image quality in terms of the signal to noise ratio (SNR), defined as the ratio between the variance of the signal to the variance of the noise (Green *et al.* 1988). We estimated the covariance matrices of the noise as in the method Min/Max Autocorrelation Factor (MFA, Switzer and Green 1984). MFA is based on the assumption that noise is much less spatially autocorrelated than the signal and, thus, calculates the covariance matrix of the noise (Σ_N) from that of the difference between the image (Z(x)) and a shift Z(x+ Δ):

$$\Sigma_\Delta = \mathrm{Cov}\{Z(x) - Z(x+\Delta)\}$$

$$\Sigma_N = 1/2\ \Sigma_\Delta$$

Then, assuming an additive noise, the covariance matrix of the signal is estimated by difference and the SNR defined from the diagonals S of the covariance matrices Σ as:

$$SNR = (S_Z - S_N)/S_N$$

In the following figure we represent SNR for the scene of fig. 9.

Click on image for full resolution

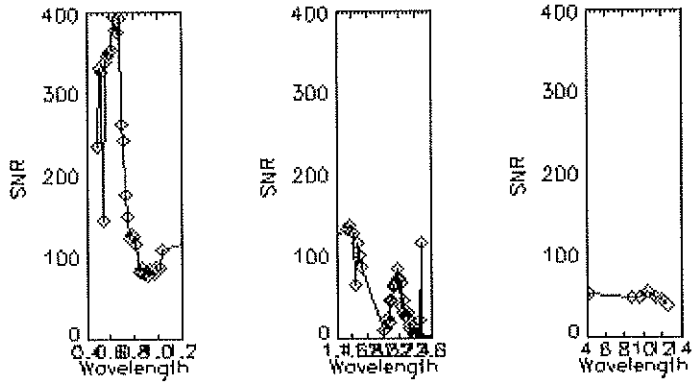

Figure 10. Signal to Noise Ratio for each DAIS band (scene represented in Fig. 9)

4.2. Atmospheric correction

In a first step, atmospheric correction has been performed using ATREM-3 (ATmospheric REMoval Program version 3; Gao, Heidebrecht and Goetz 1993) and our atmospheric measurements.

ATREM uses the 940 nm and 1140 nm regions of the spectrum and a three-channel ratioing to produce an spatially-explicit estimate of atmospheric water vapor and uses this estimate to correct the imagery for absorption in the 400 – 2500 nm region. Atmospheric scattering is calculated using 6S code (Tanre *et al.* 1986, Vermote *et al.* 1996;). The absorption of CO_2, O_3, N_2O CO, CH_4 and O_2, assumed to be spatially-uniform, are calculated using a Malkmus (1967) approach and either one of the standard LOWTRAN-7 atmospheres (Green and Gao 1993) or user-supplied vertical data (pressure, temperature and water vapor). The corrected radiance spectrum is then divided by a solar spectrum according to Green and Gao (1993) to obtain apparent reflectance. For a detailed description of the program and availability, see http://ltpwww.gsfc.nasa.gov/ltpcf/about/unix/Depotdoc/atrem/atrem.guid e2_0.ps

One problem applying ATREM to DAIS images is that DAIS lacks bands in the second (1140 nm) region of water vapor absorption, therefore only bands in and around the 940 nm absorption region can be used. Recommended values for ATREM for vegetated scenes imaged by AVIRIS are:

Table 1. ATREM water-vapor parameters for AVIRIS imagery (vegetated scenes)

	Window 1		Window 2		Absorption	
	Center (nm)	Width (# bands)	Center (nm)	Width (# bands)	Center (nm)	Width (# bands)
"940 band"	865	3	1030	3	935	5
"1140 band"	1050	3	1230	3	1130	5

which mean that:

- the 865 band, the preceeding and the following are averaged to produce an estimation of radiance not affected by water-vapor before the water vapor absorption region.
- the 1050 band, the preceeding and the following are averaged to produce a second estimation of radiance not affected by water-vapor after the water vapor absorption region.
- the 935 band, the two preceeding ones and the two following ones are used to estimate radiance affected by water vapor absorption.
- the 1130 band, the two preceeding ones and the two following ones are used for a second estimation of radiance affected by water vapor absorption.

In our case, with DAIS imagery, we run ATREM with the following parameters:

The following figures compare at-sensor radiance and ATREM-calibrated reflectance spectra for some selected targets in the p02i02c1h12_f02.bsq scene.

Click on image for full resolution.

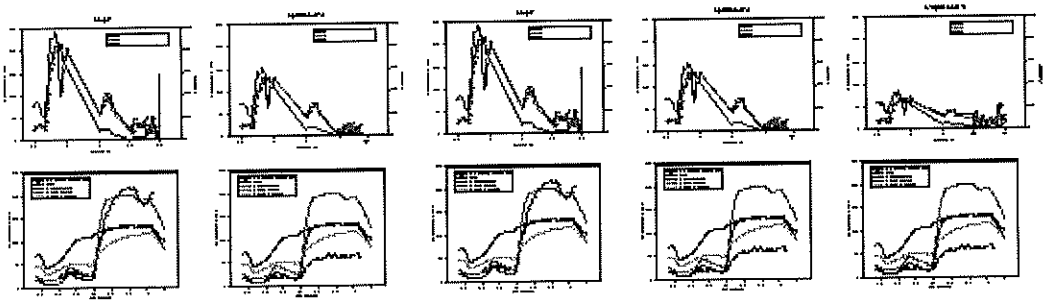

Figure 12. Spectra of selected targets.

4.2. Geometric correction

We only require an approximate geometric correction for this study, as our purpose is not using DAIS imagery for mapping but rather as a landscape-level hyperspectral tool to collect spectra of selected targets. Also, other teams have developped or are developing specific software packages intended to orthorectify airborne digital imagery that is acquired by scanning devices (a different problem than orthorectification of imagery that is acquired by still cameras). An example of these packages is PARGE (Parametric Geocoding; Schläpfer *et al.* 1988).

We have performed an approximate correction by applying an empirical polynomial that was fitted with numerous ground control points. This correction has allowed us to overlay the actual scenes on the rest of our GIS layers for the area and to select targets for detailed study.

Click on image for full resolution.

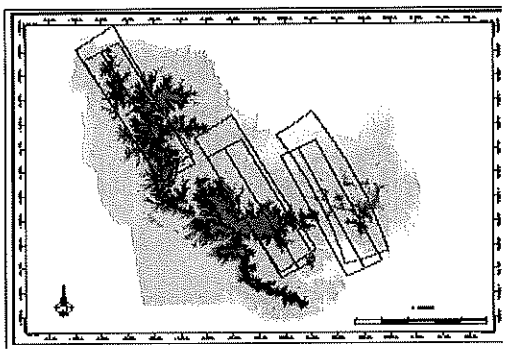

Figure 13. Planned and actually acquired scenes overlaid on the DEM.

Click on image for full resolution.

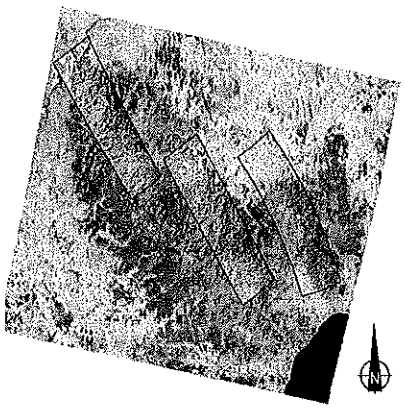

Figure 14. Overlay of DAIS color composites (Red, band 76; green, band 50; blue, band 25) on a LISS-III scene (Red, band 5; green, band 4; blue, band 2)

5. CONCLUSIONS AND NEXT STEPS

1. Although some bands present low noise/signal ratio and severe striping, bands in the 400 - 1200 nm region have a very high quality.

2. A de-striping algorithm is necessary, in particular for results with a low dynamic range (i.e., the water vapor image).

3. Excessive geometric detail is present in the water vapor image that is produced by ATREM. This is likely to be due to the fact that bands used for the water-vapor estimation include some landcover-dependent information. Also, differences in topography could be partially responsible of variations on water vapor estimates.

4. For AVIRIS, ATREM corrections include a maximum error of 2 % due to the assumption of nadir view all over the image, which in fact can have a maximum 15°; off-nadir . DAIS has a maximum 25° off-nadir view, to which airplane geometry has to be added.

5. Spectra of ATREM-calibrated reflectance seem, in principle, equivalent to the ones collected in the field, although a formal comparison will be undertaken in the second part of the project.

Our next steps, to be summarized in the final report will be the following:

1. For the atmospheric correction, we will test two more approaches (Cachorro *et al.* 1995). The first approach will be based on the formulation of Tanre et al. (1992), which will be evaluated using a simplified one-layer 6S model, with the observed values of aerosol concentration, water vapor concentration and optical depth as input. The second approach, more empirical, will use a simplification of the Tanre et al. (1992) formulation in which the scattering and gaseous transmittances are combined into observed transmittance, and where the surface albedo is also measured. This second approach is not entirely empirical as the atmospheric reflectance has to be modeled from the simplified 6S code. We will use the spectral properties of the aerosols as have been calculated for this report (Fig. 11).

2. We will use canonical analysis to assess the discriminant power of DAIS spectra.

3. Different vegetation types will be represented in the PRI - WI plane to compare with results obtained from field collected spectra.

4. Mixture analysis will be used to model DAIS spectra of complex vegetation units in terms of "pure" field-collected spectra.

If our results indicate that DAIS reflectance spectra can be modeled in terms of field-collected spectra, we will conclude that a more intensive study, flying DAIS under different vegetation status, could be undertaken to establish a routine methodology for monitoring vegetation based on hyperspectral remote sensing.

6. ACKNOWLEDGEMENTS

We are thankful to Kathy Heidebrecht for making ATREM available to us and for her help to run it properly. We also thank the DLR-DAIS processing team. The aerial campaign and image pre-processing was funded by the Large Scale Facility DAIS program of the European Union. The Fundació Catalana per la Recerca funded in part the ground campaign.

7. REFERENCES

Cachorro, V.E., Durán, P., Frutos, A.M. 1995. Caracterización del aerosol atmosférico: aplicación a las correcciones atmosféricas, In J.L. Casanova and J. Sanz (eds.) Teledetección: Usos y Aplicaciones, pp. 479-486, Univesidad de Valladolid.

Cachorro, V.E., Durán, P., Frutos, A.M., Vergaz, R. and Hernández, S., 1997. Study of the atmospheric effect on the satellite signal based on ground solar radiation measurements of high spectral resolution, In Guyot and Phulpin (eds.), *Proceedings of the Seventh Interanational Symposium on Physical Measurements and Signatures in Remote Sensing,* Courchevel, France, 7-11 April, pp. 187-192.

Gamon, J.A., Peñuelas, J., and Field, C.B., 1992. A narrow-waveband spectral index that tracks diurnal changes in photosynthetic efficiency, *Remote Sensing of Environment*, 41: 35-44.

Gao, B-C, Heidebrecht, K. B. and Goetz A. F. H., 1993. Derivation of Scaled Surface Reflectances from AVIRIS Data, *Remote Sensing of the Environment*, 44: 165-178.

Green, A., Berman, M. and Craig, M.D., 1988. A transformation for ordering multispectral data in terms of image quality with implications for noise removal, *IEEE Transactions on Geoscience and Remote Sensing,* 26(1): 65- 74.

Kneiys, F.X., Shettle, E.P. , Abreu, L.W., Chetwynd, J.H., Anderson, G.P., Gallery, W.O:, Selby, J.E.A. and Clough, S.A. 1988. Users guide to LOWTRAN-7, AFGL-TR-8-0177, United States Air Force Geophysical Laboratory, Bedford, Massachussets.

Lobo, A., 1997. Image segmentation and discriminant analysis for the identification of land cover units in ecology. *IEEE Transactions on Geoscience and Remote Sensing*, 35: 1136-1144.

Malkmus, W., 1967. Random Lorentz band model with exponential-tailed S line intensity distribution function, *Journal of the Optical Society of America*, 57: 323-329.

Peñuelas J., Filella I. 1998. Visible and near-infrared reflectance techniques for diagnosing plant physiological status. *Trends in Plant Science,* 3(4):151-156.

Schläpfer D., Meyer P., and Itten K.I., 1998: Parametric Geocoding of AVIRIS Data Using a Ground Control Point Derived Flightpath. Summaries of the Seventh JPL Airborne Earth Science Workshop, (submitted), JPL, Pasadena (CA), pp. 6. (ftp://ftp.geo.unizh.ch/pub/rsl2/paper/1998/AV_WS_98_parge.pdf).

Switzer, P. and Green, A.A., 1984. Min/Max autocorrelation factors for multivariate spatial imagery, Technical Report No. 6, Dpt. of Statistics, Stanford, 14 pp.

Switzer, P. and Ingebritsen, S.E., 1986. Ordering of time-difference data from multispectral imagery, *Remote Sensing of Environment*, 20:85-94.

Tanre, D., Deroo, C., Duhaut, P., Herman, M., Morcrette, J.J., Perbos, J. and Deschamps, P.Y., 1986. Simulation of

the Satellite Signal in the Solar Spectrum (5S), User's Guide (Laboratoire d'Optique Atmosphericque, U.S.T. de Lille, France).

Vermote, E., Tanre,D., Deuze, J.L., Herman, M. and Morcrette, J.J. 1996. Second Simulation of the Satellite Satellite Signal in the Solar Spectrum (6S), User's Guide Version 1, NASA-GSFC, Greenbelt, Maryland.